GA–A23093

ARIES-ST STUDIES

Report for the period
January 1, 1998 through December 31, 1998

by

V.S. CHAN, L.L. LAO, J.A. LEUER, Y.R. LIN-LIU,
R.L. MILLER, T.W. PETRIE, P.A. POLITZER, R. PRATER,
M.J. SCHAFFER, G.M. STAEBLER, R.D. STAMBAUGH,
A.D. TURNBULL, and W. P. WEST

APRIL 1999

GA–A23093

ARIES-ST STUDIES

Report for the period
January 1, 1998 through December 31, 1998

by

V.S. CHAN, L.L. LAO, J.A. LEUER, Y.R. LIN-LIU, R.L. MILLER, T.W. PETRIE, P.A. POLITZER, R. PRATER, M.J. SCHAFFER, G.M. STAEBLER, R.D. STAMBAUGH, A.D. TURNBULL, and W. P. WEST

This is a preprint of material sent to the University of California, San Diego for inclusion in an *ARIES-ST Report*.

Work supported by
U.S. Department of Energy
Contract No. DE-AC03-98ER54411

GENERAL ATOMICS PROJECT 30007
APRIL 1999

1. Introduction

During 1998, the General Atomics (GA) ARIES-Spherical Torus (ST) team examined several critical issues related to the physics performance of the ARIES-ST design, and a number of suggestions were made concerning possible improvements in performance. These included specification of a reference plasma equilibrium, optimization about the reference equilibrium to achieve higher beta limits, examination of three possible schemes for plasma initiation, development of a detailed scenario for ramp-up of the plasma current and pressure to its full, final operating values, an assessment of the requirement for electron confinement, and several suggestions for divertor heat flux reduction.

The reference equilibrium was generated using the TOQ code, with the specification of a 100%, self-consistent bootstrap current. The equilibrium has $\beta = 51\%$, 10% below the stability limit (a margin specified by the ARIES-ST study). In addition, a series of intermediate equilibria were defined, corresponding to the ramp-up scenario discussed below.

A study of the influence of shaping on ARIES-ST performance indicates that significant improvement in both kink and ballooning stability can be obtained by modest changes in the squareness of the plasma. In test equilibria the ballooning beta limit is increased from 58% to 67%. Also the maximum allowable plasma-wall separation for kink stability can be increased by 30%.

Three schemes were examined for noninductive plasma initiation. These are helicity injection (HICD), electron cyclotron heating (ECH)-assisted startup, and inductive startup using only the external equilibrium coils. HICD startup experiments have been done on the HIT and CDX devices. ECH-assisted startup has been demonstrated on CDX-U and DIII–D. External coil initiation is based on calculations for a proposed DIII–D experiment. In all cases, plasma initiation and preparation of an approximately 0.3 MA plasma for ARIES-ST appears entirely feasible.

A rampup scenario for increasing the current from 0.3 MA to the final 31 MA was developed. In order to avoid axisymmetric instabilities, the discharge starts with a small, approximately circular cross-section, limited at the outboard side (see figures). The minor radius is increased (and aspect ratio is reduced) until the plasma fills the width of the reactor (at about 10 MA current). Subsequently the elongation is raised to the final value of 3.4. If the confinement is assumed to be standard H–mode throughout, a peak power of 120 MW is needed. Restricting the external power to 50 MW leads to a requirement for confinement control, raising the confinement multiplier by as much as 50% over H–mode during the ramp-up. Most of the current is provided by bootstrap current (rising from 50% at the start of the ramp to 100% at the end).

A brief transport analysis showed that, if the ion thermal transport is assumed to behave neoclassically, the ignition condition is maintained if the electron thermal diffusivity exceeds the ion value by a factor of 150–500, depending on the density profile. The lower value is found for the profiles being used in the ARIES-ST study.

The peak heat flux on the inboard and outboard divertors for the 529 MW ‘‘Strawman’’ case has been estimated to be well above the handling capabilities of present day cooling technology. Two specific methods of reducing the peak flux are outlined. The most straightforward of the two is tilting the wetted surfaces with respect to the divertor separatrix flux surface. The second method assumes that the double-null ARIES-ST core plasma can run close to (or on) the centerpost without an observable adverse effect on energy confinement. Moving the core plasma closer to the centerpost can reduce (perhaps, eliminate) power flow along the inboard SOL and, if the separatrix flux surface is limited on the centerpost, power flow to the outboard divertors also can be reduced. Our estimates of divertor and upstream (midplane) plasma density based on simple 1-D transport modelling suggest that plasma temperatures in the SOL and divertors are at least in a range that allows one to make a plausible argument for minimizing the effect of sputtering in ARIES-ST.

The results of this work were presented at an ARIES-ST team meeting at Princeton Plasma Physics Laboratory (PPPL) in September 1998, and also at the International Atomic Energy Agency Technical Committee Meeting on Spherical Tokamaks at the University of Tokyo in October 1998.

2. Magnetohydrodynamics (MHD)

2.1. β Optimization of the Spherical Torus [2-1]

For the ST, the interest lies in fully optimizing the cross-section against ideal ballooning, axisymmetric, and low to moderate n kink modes. The optimization proceeded along the same lines as in Refs. 2-2 and 2-3. For a fixed cross-section, the equilibrium and ballooning stability were iterated with $C_{\rm b}$ fixed at unity to enforce bootstrap alignment, and the parameter p_0 increased until marginal ballooning stability was reached at some point in the profile. Note that, in contrast to the conventional aspect ratio studies, the entire cross-section was considered. The pressure profile was chosen as

$$J_{\rm s}(\psi) = J_0\left(1-\psi^{\mu}\right)^2 \ , \tag{2-1}$$

with $d_{\rm p}=0$ to eliminate the pressure pedestal, and with $g(\psi)$ fixed at the optimum obtained in Refs. 2-2 and 2-3; namely with $N=4$ and the coefficients $a_0=0.025$, $a_1=a_2=0$, $a_3=0.975$, and $a_4=-1$. The seed current in Eq. (2-1) is always negligible except near the axis, but J_0 was used to adjust q_0. Once the ballooning optimized equilibrium was constructed, the axisymmetric $n=0$ and low $n\geq 1$ kink stability were determined by finding the conformal wall position required to obtain marginal stability for each n.

The previously published results in Refs. 2-2 and 2-3 at $R/a=1.4$ found an optimum at $\beta=54\%$ with $\kappa=3.0$, which was the highest elongation considered, $\delta=0.5$, and a broad pressure profile. In the present study, the aspect ratio, elongation, and triangularity were fixed at $R/a=1.6$, $\kappa=3.4$, and $\delta=0.6$, respectively, and only the squareness ζ was varied. The reasoning behind these choices was based largely on the prior experience of Refs. 2-2 and 2-3, and is explained in detail in Ref. 2-4. For the present purpose, we note only that the change in R/a is minor and that the present results have improved on the previous optimization [2-2,2-3] by increasing κ and δ, and by optimizing over the squareness ζ.

The starting point was then a configuration with $R/a=1.6$, $\kappa=3.4$, $\delta=0.6$, and $\zeta=0$, which resulted in a volume averaged β of 58% and $\beta_{\rm N}=8.4$. This had 99.7% bootstrap fraction and was stable to $n=0$ axisymmetric modes with a wall at $\lambda_{\rm w}=0.65$. Here, $\lambda_{\rm w}=1-R_{\rm w}/a$ is the conformal wall distance with $R_{\rm w}$ the wall minor radius at the midplane. The marginal $n=1$, 2, and 3 ideal kink modes each required a wall at $\lambda_{\rm w}=0.3$. This case then served as a basis for investigation of the effect of varying ζ. For these calculations, the effects of inboard and outboard squareness $\zeta_{\rm i}$ and $\zeta_{\rm o}$ were considered independently.

The dependence of the ballooning optimized β limits on ζ_i and ζ_o is summarized in Fig. 2-1. Four cases were considered: varying ζ_i with $\zeta_o = 0$, varying ζ_o with $\zeta_i = 0$, varying $\zeta_i = \zeta_o$, and varying ζ_o with ζ_i fixed at -0.2. The base case then corresponds to the point at which the first three curves intersect where $\zeta_i = \zeta_o = 0$ and $\beta = 58\%$. The inset in Fig. 2-1 shows the $\zeta = 0$ configuration overlaid with the cross-section for $\zeta_i = -0.2$ and $\zeta_o = +0.1$.

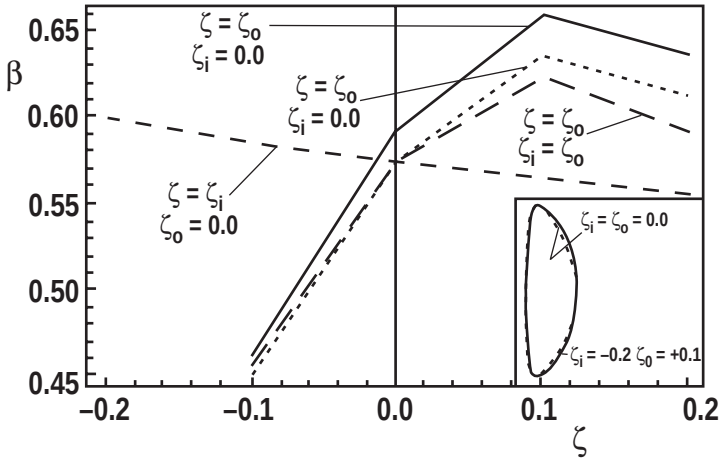

FIG. 2-1. Ballooning optimized β limits as a function of ζ_i and ζ_o for the ST. Shown are curves for varying ζ_o at $\zeta_i = 0$ (dotted), varying ζ_i at $\zeta_o = 0$ (broken curve), varying $\zeta_i = \zeta_o$ (long dashes), and varying ζ_i with ζ_o fixed at -0.2 (solid curve). The inset shows a comparison of the cross-section shapes for the ST standard DEE with $\zeta_i = \zeta_o = 0$ (dashed) and the optimized ST with $\zeta_i = -0.2$ and $\zeta_o = +0.1$ (solid).

Moderate positive squareness on the outboard side provides a clear improvement in the ballooning optimized β limit, with the optimum at $\zeta_o \sim 0.1$. The increase is quite substantial, leading to an increase in β of 7% for $\zeta_i = \zeta_o$ and 8.5% for $\zeta_i = 0$. The inboard squareness has a weaker effect but an increase of a few percent in β is still possible by taking $\zeta_i = -0.2$ with no outboard squareness.

Combining the benefits of negative inboard squareness with moderate positive outboard squareness further enhances the optimum β limit and the enhancement appears to be roughly additive. This is shown by the last curve where ζ_i has been fixed at -0.2 and the resulting optimum at $\zeta_o = +0.1$ has $\beta = 67\%$, which is a relative increase in β of 15% over the base case, or 9% in absolute β. β_N was also increased by 5% to 8.8. Since [2-2,2-3] $\beta\beta_p \simeq \beta_N^2\{1+[(\kappa^2+1)/2]f(\delta,\zeta)\}$, and β_p remained essentially unchanged, this indicates that most of the increase in β results directly from the increase in β_N. This increase in β is clearly significant, considering the relatively low values of $|\zeta|$ required to obtain it, and especially in view of the resulting small changes in the actual cross-section shape shown in Fig. 2-1.

The axisymmetric and low n kink stability limits are also improved by the optimization of ζ_i and ζ_o. For the new optimum, the axisymmetric marginal wall position is extended to

$\lambda_w = 0.85$ compared to the case with $\zeta = 0$ for which $\lambda_w = 0.65$. The $n = 1$, 2, and 3 marginal wall points are essentially unchanged within the accuracy to which the marginal points can be determined ($\lambda_w \simeq 0.3 \pm 0.05$). The $n = 4$ and $n = 5$ stability limits were also found to be within this range. This represents a definite improvement in the stability, however, since β is substantially higher than the base case with $\zeta = 0$. The optimization over ζ_i and ζ_o has effectively improved the ballooning and low n kink β limits by the same magnitude. The even greater improvement in axisymmetric stability is not unexpected since the $n = 0$ modes are not destabilized by increasing β; increasing β even tends to be mildly stabilizing.

This magnitude improvement is typical of changes in the triangularity δ of the same order. However, such a change in δ would result in a much more noticeable change in cross-sections than that in Fig. 2-1 and preliminary indications are that it would require significantly larger changes in the coil currents to effect such a change.

The limiting modes will be discussed in more detail in a subsequent paper [2-4]. However, it is sufficient to note here that there is no striking difference in the unstable modes between the equilibria with and without squareness. In each case, the axisymmetric modes have a strong vertical shift component but with large distortions near the edge, and the unstable kink modes exhibit a strong ballooning character and are located mostly in the outer half of the cross-section. The differences occur in relatively subtle changes in the relative amplitudes of the various poloidal harmonics.

2.2. Rigid Body Vertical Stability of ARIES-ST

Summary

The ARIES-ST EFIT equilibrium studied (800623) is very stable to rigid body vertical motion. In essence, the conducting wall required to stabilize vertical motion can be placed very far from the plasma before control becomes an issue. This is a consequence of two properties of the equilibrium. First, the plasma configuration is close to the ‘‘natural plasma’’ shape, *i.e.*, plasma shape associated with a purely vertical vacuum field. This type plasma is neutral to plasma vertical motion and, in theory, needs no conducting wall. Second, the current density profile is strongly peaked near the outer extreme of the plasma. At this location, the current strongly couples with outer conducting shells to retard plasma motion. Reasonable passive stability growth rates are seen for a wall at a $R_{wall}/a \sim 2$ even with 50% outer poloidal coverage. For a closely fitting wall similar to that in DIII–D ($R_{wall}/a \sim 1.2$), the inductive stability parameter is $f \approx 6$, where $f \to 1$ results in motion on the Alfvén time scale. Using a 2 cm shell of Inconel covering the outer poloidal half of the plasma, the growth rate is of order $\gamma \sim 10$ s^{-1}. By comparison, DIII–D can routinely operate with $f < 2$ and $\gamma > 100$ s^{-1}. Other stability limits, most notably kink or resistive wall mode stability, are expected to be more restrictive than vertical stability. In addition, other equilibrium points of the plasma evolution should be checked for vertical stability

properties, since different current density profiles and vacuum fields can lead to more restrictive requirements.

Rigid Body Vertical Stability Problem

Highly elongated plasmas are typically vertically unstable. That is, for a small vertical displacement, the force on the plasma from the poloidal field (PF) coils is in the same direction as the displacement. Any vertical perturbation of the plasma tends to grow exponentially. Axisymmetric resistive conductors located close to the plasma (like the DIII–D vacuum vessel) retard this motion through eddy currents induced in the wall by the plasma motion. An estimate of the vertical stability of the system can be obtained by rigidly shifting the plasma and determining the resulting system response [2-5]. A sufficiently coupled axisymmetric shell can slow the Alfvén scale vertical motion to a time scale characterized by the L/R time of the shell. The inductive stability parameter f is a measure of how close the system is to Alfvén timescale motion. The growth rate of the vertical instability γ is inversely proportional to the stability parameter [2-5]:

$$\gamma = \frac{1}{\tau_{\text{shell}}} \frac{1}{(f-1)} , \tag{2-2}$$

where τ_{shell} is the time constant associated with currents in the shell produced by an instantaneous rigid shift of the plasma. The inductive stability parameter depends on the mutual inductance between the plasma, PF coils, and passive structure; a matrix formulation is presented in Ref. 2-5.

In the above formula, the growth rate approaches infinity as the stability parameter approaches one. As f approaches 1, plasma inertia begins to become important and the formula is not longer valid.

Two independent codes are used in this analysis: ASTAB, a Fortran-based code for passive and active stability analysis; and ZRIG, a MATLAB routine for passive analysis. Both codes predict the eigenmodes of the system and agreement between models is within 1%. Both codes have been benchmarked against DIII–D results and produce good predictions for systems with stability parameter much larger tan one. For systems with stability parameter close to one, nonrigid plasma motion can dominate the stability properties and the rigid model is no longer valid.

Equilibrium / Current Density / Vacuum Field Characteristics

An EFIT equilibrium (800623.00210) is used in this study. Figure 2-2 shows the equilibrium, flux contours, and associated parameters [2-6]. This is a highly elongated plasma with moderate triangularity and peaked current profile. Figure 2-3 shows the current density distribution over the plasma. Notice the large peaking near the outer extreme of the plasma. This outer current will strongly react with any external conductive structure to

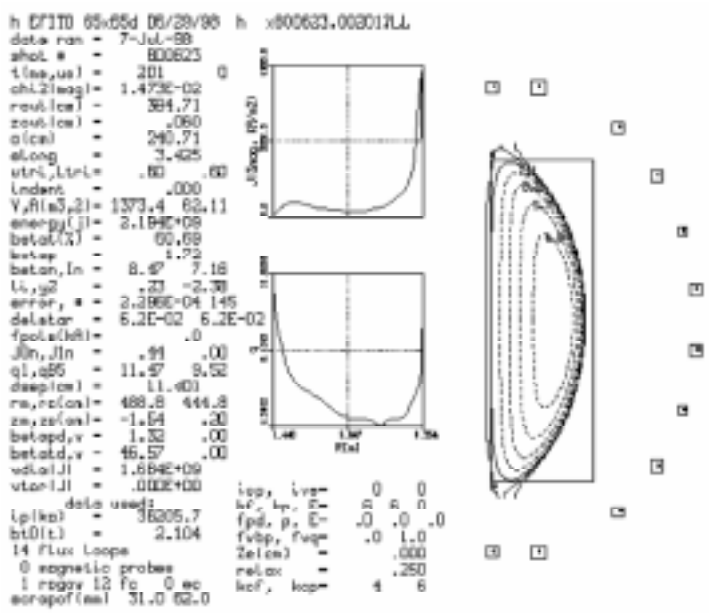

FIG. 2-2. ARIES-ST EFIT equilibrium.

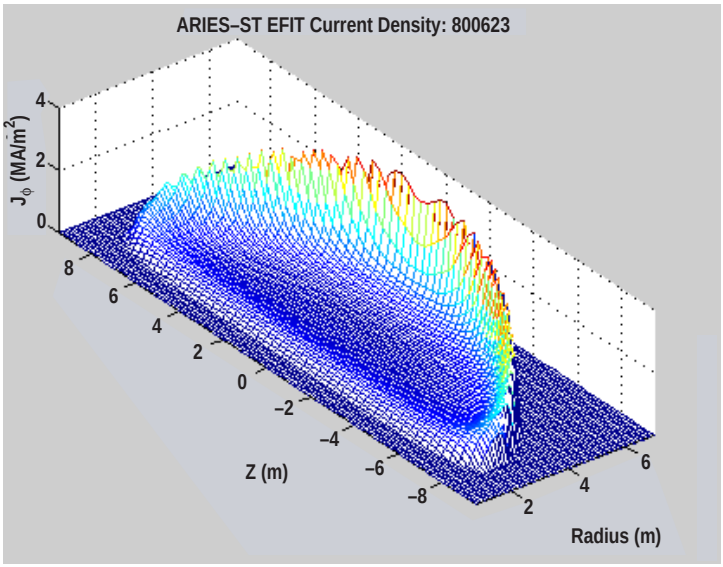

FIG. 2-3. ARIES-ST current density distribution.

greatly retard plasma vertical motion. The low current on the inside of the plasma indicates that passive structure located near the inside of the machine will have little influence on vertical stability.

Figure 2-4 shows the vacuum field flux plot. The field is very close to a uniform vertical field. A pure vertical field produces the so-called ‘‘natural’’ plasma shape [2-7]. A plasma in a uniform vertical field is neutrally stable to vertical displacements. In theory, a

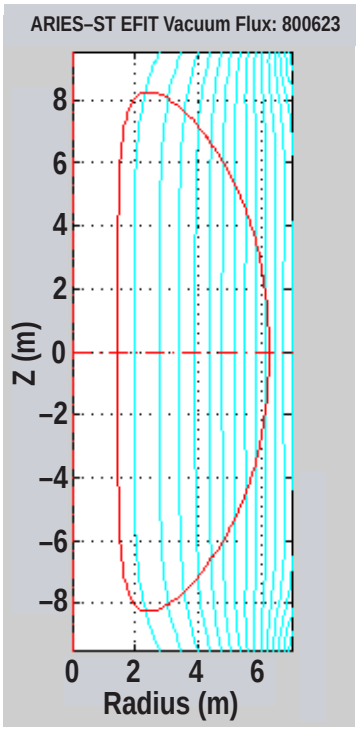

FIG. 2-4. ARIES-ST vacuum flux field. Note that the field is almost vertical which would correspond to the natural shape.

naturally elongated plasma is neutrally stable to vertical motion without a passive wall. The slight concave curvature of the lines, especially near the X–points, indicates that there is a destabilizing force. However, it is very small when compared to that found in a moderate aspect ratio tokamak, or in a spherical tokamak with a broader current density profile. Since this destabilizing force is driving the vertical instability, passive stabilization of the system should be relatively easy.

Rigid Body Vertical Analysis

Figure 2-5 shows the vertical stability parameters for a full shell placed around the plasma at 1.2 times the minor radius ($R_{\text{wall}}/a = 1.2$). The shell is modeled using 80 axisymmetric elements. The wall thickness is 2 cm and the material is Inconel 625 with a resistivity of $\rho = 1.3\,\mu\Omega$-m, which corresponds to a conductivity of approximately 1% pure copper (DIII–D vacuum vessel material). The PF coils are not included as part of the passive system and inclusion would make the system more stable.

For a close fitting shell ($R_{\text{wall}}/a = 1.2$), the stability parameter is greater than six indicating that the system is far from the stability limit ($f \sim 1$). The vertical growth rate is 6.5 s^{-1} ($\tau \sim 160$ ms) which is a very low value for an Inconel stabilized system. These results are expected based on the near vertical equilibrium field and large outward shift of the plasma current. For comparison, DIII–D routinely operates with a stability factor below two

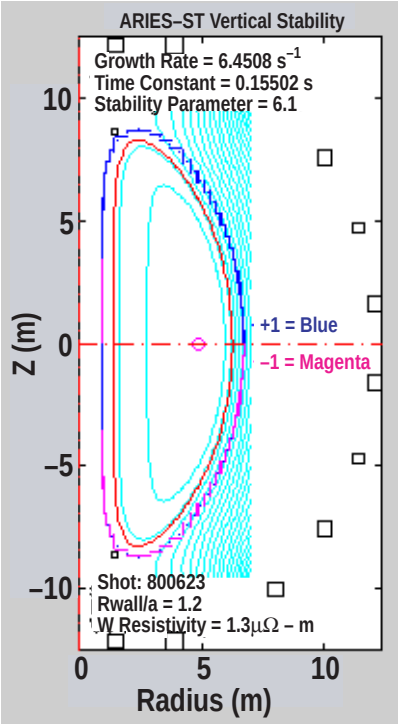

FIG. 2-5. ARIES-ST rigid body vertical stability properties for 100% coverage at $R_{\text{wall}} / a = 1.2$. Two element colors represent direction of current associated with unstable eigenmode.

and has operated without loss of control at stability factors below 1.1. In such cases, DIII–D operates with growth rates in excess of 500 s^{-1} ($\tau \sim 2$ ms).

With the plasma current peaking near the outer wall, the inner passive wall provides little help in stabilizing the plasma. Figure 2-6 shows the layout of several cases studied with varying shell to plasma distance and approximately 50% outer wall coverage. Table 2-1 shows the results. For comparison, column 1 and 2 show the 100% and 50% coverage results for the $R_{\text{wall}} / a = 1.2$ case. Removal of the inner wall has little influence on the stability properties. As the wall is moved away from the plasma (remaining columns in the table), the stability parameter drops and the growth rate increases. The marginal stability point ($f \rightarrow 1$) is approximately $R_{\text{wall}} / a = 2.5$. The benign vertical stability properties of this equilibrium allows for a wide range of stabilization options. For this equilibrium, it is expected that other requirements, more notably kink or resistive wall mode stability, will be more restrictive in defining the stabilizing wall requirements.

It should be noted that other intermediary equilibria may be much more unstable than this highly optimized equilibrium. Higher internal inductance plasmas with smaller current density shifts needed during the plasma initiation are expected to be less robust to vertical stability. All equilibria needed to establish this final plasma should therefore be tested for vertical stability.

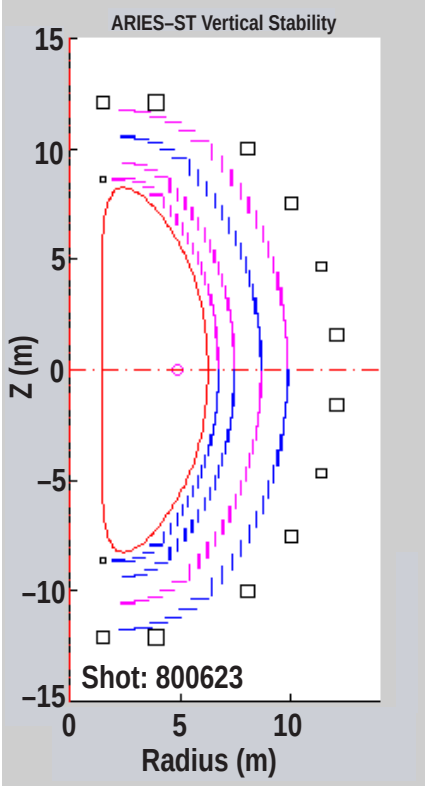

FIG. 2-6. Wall position for 50% outer wall coverage and for different wall to plasma distances: $R_{\text{wall}} / a = 1.2,\ 1.5,\ 2.0,$ and 2.5.

Table 2-1
Rigid body vertical stability parameters for ARIES-ST

Wall coverage	100%	Outer 50% (see Fig. 2-6)			
R_{wall} / a	1.2	1.2	1.5	2.0	2.5
Stability parameter f	6.10	6.05	3.85	2.10	1.14
Growth rate γ (s–1)	6.45	6.61	10.8	26.4	175
Time constant τ (ms)	155	151	92	38	5.7

References for Section 2

[2-1] A.D. Turnbull *et al.*, ‘‘Improved MHD Stability Through Optimization of Higher Order Moments in Cross-Section Shape of Tokamaks,’’ to be published in Physics of Plasmas (1999).

[2-2] R.L. Miller *et al.*, Phys. Plasmas **4**, 1062 (1997).

[2-3] R.L. Miller *et al.*, in Proc. Joint Varenna-Lausanne International Workshop on Theory of Fusion Plasmas (Varenna, 1996) (Editrice Compositori Bologna), p. 17.

[2-4] A.D. Turnbull, R.L. Miller, Y.R. Lin-Liu, and T.S. Taylor, ‘‘MHD Stability Optimization of the Cross-Section of a Spherical Torus,’’ in preparation.

[2-5] J.A. Leuer, Fusion Technol. **15**, 489 (1989).

[2-6] L.L. Lao, General Atomics, personal communication (1998).

[2-7] J.A. Leuer, General Atomics, personal communication (1996).

3. Current Initiation

3.1. Inductive Startup

Techniques to initiate and ramp up the plasma current to full values without a center solenoid are required for ARIES-ST. RF, neutral beam and bootstrap current drive techniques appear to have potential for current ramp after a certain level of current has been established by some other technique [3-1]. Plasma current can be initiated and ramped up to modest values using the induction available from the PF coils located near the centerpost above and below the vacuum vessel (herein called the divertor coils). Time dependent MHD modeling of plasma startup using the divertor coils on DIII–D is being carried out in collaboration with R. Khayrutdinov of TRINITI labs, using the DINA code. Preliminary results were presented at the STWS97, St. Petersburg. This work has indicated several issues which should be addressed when evaluating the capability of the PF coil design to provide plasma startup. These issues include not only the volt second and loop voltage capability of the divertor coils and power supplies, but also the vertical and horizontal control of the plasma column during ramp up and the formation of a good null prior to breakdown.

Maintaining vertical position stability during plasma startup is likely to limit the divertor coil currents and also the available loop voltage and volt seconds. Previous work on DIII–D using electron cyclotron heating (ECH) preionization and heating [3-2] has shown very reliable low voltage breakdown and ramp up. With an ECH (fundamental heating, high field side launch) power of about 650 kW applied continuously throughout the initiation and ramp up, important results from this paper are:

- Reliable initiation and ramp up achieved with the loop voltage as low as 1.6 V (electric field about 0.15 V/m).
- Reliable initiation and ramp up achieved with large error fields and no null present in the vessel.
- Current channel appeared to initiate near the center of the vessel. Location of the resonance was not important.
- In this experiment, elongation was kept below 1.3 for the duration of the rampup.
- All else being constant, the current ramp rate was a linear function of the loop voltage.

To first order we should be able to scale the various inductive and resistive components of the loop voltages calculated from the DIII–D data to ARIES-ST. Following Lloyd *et al.* [3-2], the plasma current ramp rate is given by

$$\frac{dI_p}{dt} = \frac{V_l - [V_{res} + 0.51 I_p d(L_i + L_a)/dt]}{L_i + L_a} , \quad (3\text{-}1)$$

where V_l is the loop voltage, L_i is the internal inductance, L_a is the annular inductance, and V_{res} is the resistive voltage from the plasma current. Assuming the current channel profile shapes to be the same in both cases, and assuming whatever ECH heating mode is chosen will produce the same plasma parameters as the fundamental heating on DIII–D, then the inductances and the resistive voltages will scale with the major radius of the center of the current channel. Assuming that on ARIES-ST we position the current channel in the outer part of the vessel, $R_{ARIES-ST} \approx 4.95$ and $R_{DIII-D} \approx 1.7$, the inductances derived for the DIII–D ECH assisted startup are given in Table 3-1, with the values scaled to the expected radius for ARIES-ST.

Table 3-1
ARIES-ST inductances and loop voltages scaled from DIII–D assisted startup data

DIII–D	ARIES-ST
$L_i \approx 0.5\mu H$	$L_i \approx 1.46\mu H$
$L_a \approx 0.3\mu H$	$L_a \approx 0.87\mu H$
$V_{res} \approx 0.8 V \quad (E \approx 0.075 V/m)$	$V_{res} \approx 2.33 V \quad (E \approx 0.075 V/m)$
$0.5 I_p d(L_i + L_a)/dt \approx 0.15 V$	$0.5 I_p d(L_i + L_a)/dt \approx 0.44 V$

From Eq. (3-1), at a loop voltage of 5.0 V, a current ramp rate of 1.0 MA/s would be achieved on ARIES-ST. To ramp to a plasma current of 0.1 MA would take 100 ms and 0.5 Vs.

The ten PF coil set used in the EFIT equilibrium model 800708.00200 for ARIES-ST [3-3] appears to be more than adequate to provide the needed inductive drive. To achieve the triangularity and elongation required to meet the steady-state plasma performance, the divertor coil pairs (1 and 6, and 2 and 7) must be designed to carry 32 and 15 MA, respectively. PF coil positions and currents [3-4] and the resulting fields and flux at the proposed location of the current channel during rampup are given in Table 3-2. These calculations indicate that a net current swing of less than 1.5 MA distributed judiciously between these two divertor coil pairs will provide the required 0.5 Vs. Thus, some freedom is left in choosing the PF coil currents for achieving a reasonable null prior to breakdown, and for maintaining positional stability.

To provide assurance that breakdown can be achieved reliably and ensure a minimum of resistive volt second consumption, ECH power at the fundamental frequency at $R = 4.95$ m should be provided. Power requirements have not been estimated, but are probably modest.

Table 3-2
PF coil positions and currents for ARIES equilibrium 800708.00200
and the fields and flux at $R = 4.95$ and $Z = 0$

Coil No.	R_{coil} (m)	Z_{coil} (m)	I_{coil} (m)	B_r (T)	B_z (T)	Flux (Wb)
1	2.0	10.5	31.13	–0.028	0.036	3.76
2	3.0	10.5	–14.45	0.027	–0.037	–3.75
3	10.5	7.5	–26.52	0.30	–0.77	–62.88
4	10.5	6.3	26.06	–0.34	0.92	73.56
5	10.5	4.3	–16.42	0.24	–0.79	–60.77
6	2.0	–10.5	31.66	0.028	0.037	3.83
7	3.0	–10.5	–14.48	–0.027	–0.037	–3.75
8	10.5	–7.5	–27.48	–0.31	–0.80	–65.15
9	10.5	–6.3	26.56	0.34	0.94	74.98
10	10.5	–4.3	–16.04	–0.24	–0.78	–59.34

Some detailed studies are suggested in the next design phase. Most important, a time dependent MHD model of ramp up should be developed, to ensure adequate position control during early phases. Pre-bias currents on the divertor coils may result in vertical or horizontal instabilities at low plasma current, which will stress the control system. The outer PF coils must be used to provide both a reasonable null prior to breakdown and positional control. The large distance between the PF coils and the plasma column will enhance the control problems. Placing the plasma column near the outer wall will provide some passive stabilization.

3.2 ECH Startup

A means of generating the plasma current in ARIES-ST must be developed since there is no Ohmic heating coil in this conceptual device. The approach is to use bootstrap current overdrive to generate most of the current. However, this approach is not effective unless there is already sufficient plasma current that flux surfaces are closed and trapped electrons are present. Studies reported elsewhere in this document show that this condition requires about 250 kA of plasma current. In this section, a means of generating this seed current using ECH is presented.

The approach to ECH startup is to follow the technique developed on the CDX-U device [3-5], a small tokamak with low aspect ratio (1.3). This device has a major radius of 0.43 m, minor radius of 0.33 m, and toroidal field on axis of 0.03 T. The toroidal field, of course, falls in proportion to the major radius, so that at a radius of 0.15 m the file is 0.087 T. This field corresponds to an electron cyclotron resonance frequency of 2.45 GHz. In the CDX-U experiments, rf power at this frequency is applied with power in the range 1 to

10 kW. In addition to the toroidal field in CDX-U, a vertical magnetic field with strong convex curvature is applied. This geometry is shown in Fig. 3-1. The toroidal plasma current which appears is detected by means of magnetic probes installed at the vacuum boundary.

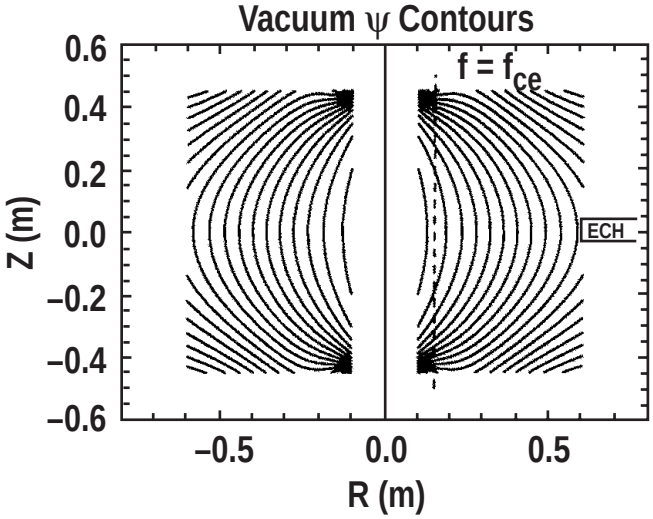

FIG. 3-1. The vacuum poloidal flux contours for CDX-U, taken from Ref. 3-6.

In these experiments on CDX-U, plasma current was found when the ECH was applied. The detailed observations include:

- The plasma current is linearly proportional to the applied power. For 8 kW of power, up to 1 kA of current was found, depending on other parameters.
- The plasma current is maximum at lower neutral pressure, with moderately strong dependence. Pressures of $1–2\times10^{-5}$ Torr were optimum.
- The plasma current is only weakly dependent on the magnitude of the vertical field. No changes in the curvature of this field were possible.
- The plasma current increases as the radius R_{res} of the resonant surface decreases.
- The plasma density increases to above the cutoff density for ECH.
- Under good conditions closed nested flux surfaces can be generated. This geometry is identical to that of an ordinary tokamak with high q (safety factor.
- The center of the closed flux surfaces and the peak of the density occur at a major radius corresponding to the second harmonic of the applied frequency.

The flux surfaces which form due to the plasma current are shown in Fig. 3-2. The origin of the observed current is attributed by the CDX-U group to Pfirsch-Schlüter currents,

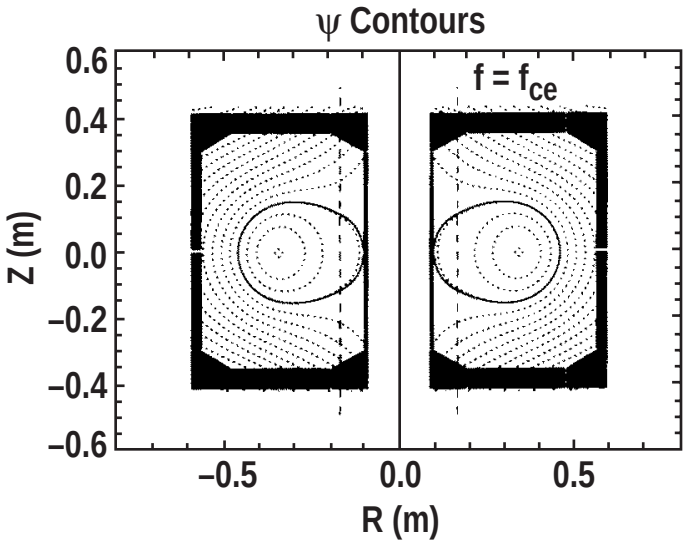

FIG. 3-2. The flux contours in CDX-U as determined from measurements of the magnetic field at the vacuum boundary, from Ref. 3-6.

which flow unidirectionally in a configuration with open field lines, and to the effect of electrons precessing toroidally due to the curvature of the vertical field. These effects are believed strong enough, under good conditions, to generate closed flux surfaces and a tokamak-like geometry. When this occurs, both effects no longer generate current due to the canceling effects which take place on the inside and outside of a flux surface. However, if the β_p (poloidal beta) is large enough, the bootstrap current fraction will be large, and this neoclassical effect can cause the current to continue to increase.

This experiment was repeated sketchily on DIII–D in 1993. About 1 MW of power at 60 GHz was applied to a vacuum configuration of toroidal field plus a convex curved vertical field. Plasma currents up to 25 kA were produced, although for the configuration in DIII–D this current was insufficient to generate closed flux surfaces.

This approach may be applied to ARIES-ST, which has a vacuum toroidal field of 1.85 T at a major radius of 3.22 m, with a minor radius of 2.01 m. The radius of the inner wall is therefore 1.21 m. Following the CDX-U results, we set the major radius of the resonance to be a short distance of order 30 cm outboard of the inner wall. At a major radius of 1.52 m, the toroidal field is 3.93 T, which corresponds to a fundamental cyclotron resonance frequency of 110 GHz, a frequency at which high power is available now. The ordinary mode has a cutoff at a density of 1.5×10^{20} m^{-3}, which is not a limitation for startup activities. The second harmonic occurs at a major radius of about 3 m, near the center of ARIES-ST. The ordinary mode is poorly absorbed at the second harmonic, but the extraordinary mode is accessible up to densities near the cutoff at 0.75×10^{20} m^{-3}, and absorption is strong. It seems that 110 GHz power is ideally suited for startup on ARIES-

ST. However, for this approach to be applicable, a vertical field with moderately strong curvature must be possible during the startup phase, similar to that in Fig. 3-1.

Wave absorption is an issue. Figure 3-3 shows the optical depth [the optical depth t is defined as $P_A = P_0(1 - e^{-t})$, where P_A is the absorbed power and P_0 is the incident power] for the fundamental O–mode and Fig. 3-4 shows it for the second harmonic X–mode. Absorption at the fundamental resonance by the O–mode takes place due to finite Larmor radius effects, and at very low temperature this effect is very small. Hence, it would not seem to be an effective approach to breakdown. Theories of breakdown usually assume that the wave polarization is scrambled by multiple reflections at the vessel walls, and some power appears as X–mode power propagating from the high field side. This power is absorbed both at the cyclotron resonance and at the nearby (at low density) upper hybrid layer. This presumably starts the breakdown process and brings the plasma parameters to a range where the O–mode is at least partially absorbed, at around a temperature of a few hundred eV and a density of 10^{19} m^{-3}. As the temperature rises at constant density, the absorption increasing leading to a rapid increase in temperature.

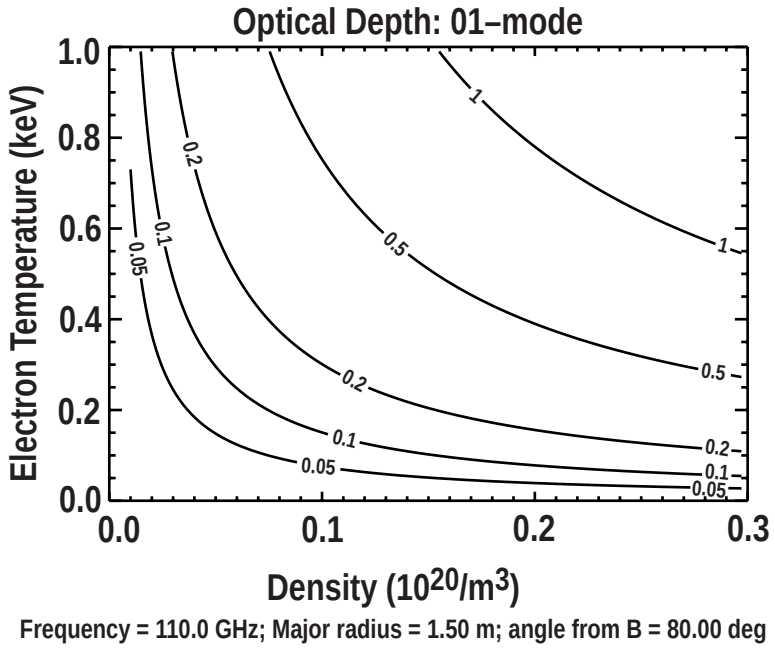

FIG. 3-3. Optical depth for the fundamental ordinary mode, as a function of electron temperature and plasma density, for ARIES-ST parameters of major radius of the fundamental resonance of 1.5 m for 110 GHz power.

As the temperature rises, the absorption shifts to the location of the second harmonic resonance, as the CDX-U data shows. The absorption is much stronger for the second harmonic X–mode as Fig. 3-3 shows. Nearly full single pass absorption takes place for temperatures above a few hundred eV. Since the waves are incident from the high field side, they encounter this second harmonic resonance first and are well absorbed there.

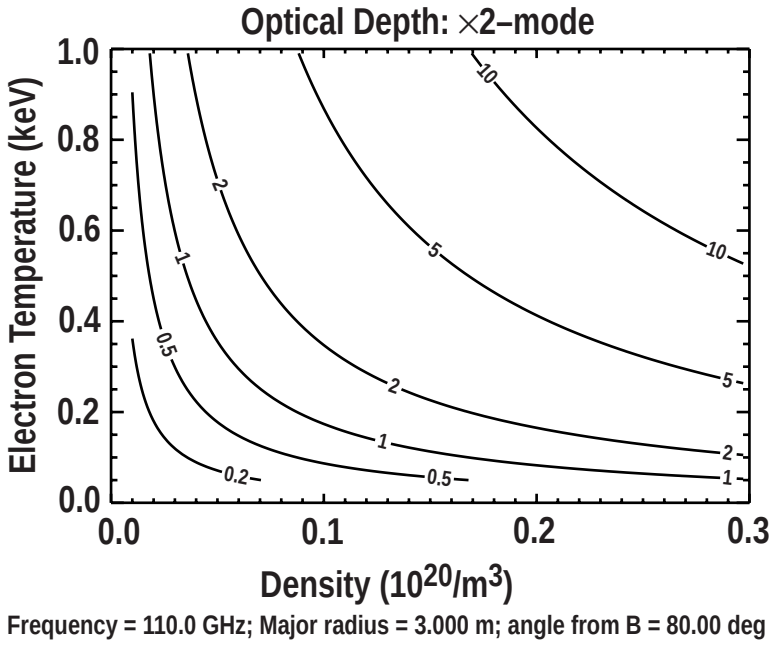

Fig. 3-4. Same as Fig. 3-3, but for second harmonic X–mode.

A key question is how much power is required for startup. An estimate can be made by scaling the required power by the plasma current, using the linear relationship between current and will power found in the CDX-U experiments. The power required should also increase linearly with the major radius, on the basis that the larger the major radius, the smaller the stacking factor due to electron recirculation. Then, $P_{\mathrm{ECH}} = c\, I_{\mathrm{p}}\, R_0$ and from CDX-U the value of c is 24 W/A-m. Scaling to DIII–D as a check point, using this value for c and a current of 25 kA, gives a required power of 0.96 MW, in good agreement with the experimental value. Scaling to ARIES-ST, with 250 kA and a major radius of 3.22 m, gives 19 MW. This level of power is not unreasonable, and electron heating power of this magnitude will be needed for the bootstrap ramp up anyway.

In summary, it appears that ECH startup techniques may be expected to generate enough current to create closed flux surfaces, at which point bootstrap ramp up can take over. The power required to generate this current is of the same order as that needed for the bootstrap ramp up.

References for Section 3

[3-1] P.A. Politzer, ARIES-ST meeting, July 1998.

[3-2] B. Lloyd *et al.*, Nuclear Fusion **31**, 2031 (1991).

[3-3] L.L. Lao, General Atomics, private communication (1998).

[3-4] J.A. Leuer, General Atomics, private communication (1998).

[3-5] C.B. Forest, Y.S. Hwany, M. Ono, and D.S. Darrow, Phys. Rev. Lett. **68**, 3559 (1992).

4. Current Rampup Using Bootstrap Overdrive

4.1. Introduction

A rampup scenario for increasing the current from 0.3 MA to the final 31 MA was developed. In order to avoid axisymmetric instabilities, the discharge starts with a small, approximately circular cross-section, limited at the outboard side (Fig. 4-1). The minor radius is increased (and aspect ratio is reduced) until the plasma fills the width of the reactor (at about 10 MA current). Subsequently the elongation is raised to the final value of 3.4. If the confinement is assumed to be standard H–mode throughout, a peak power of 120 MW is needed. Restricting the external power to 50 MW leads to a requirement for confinement control, raising the confinement multiplier by as much as 50% over H–mode during the rampup. Most of the current is provided by bootstrap current (rising from 509% at the start of the ramp to 100% at the end).

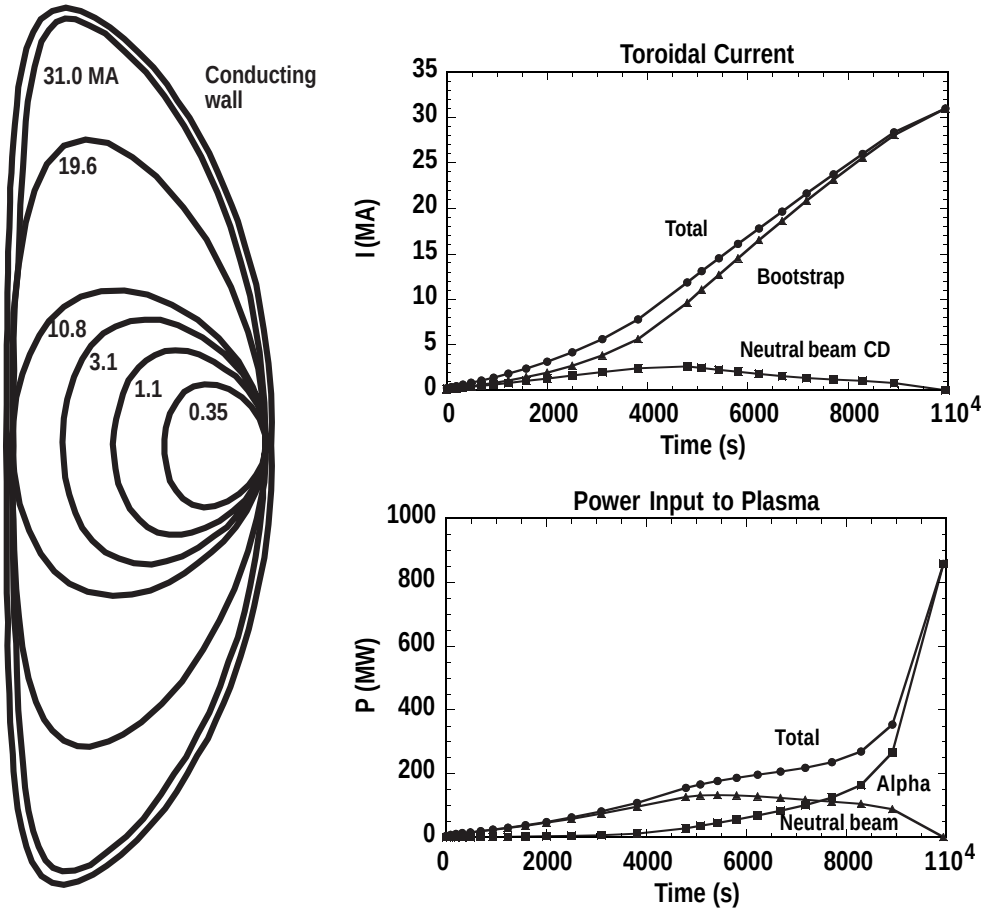

FIG. 4-1. Evolution of plasma shape, current, and power (total, alpha, and neutral beam) during ramp-up.

4.2. Ramp-up Strategy

After analysis of several ramp-up. Instead of ramping the elongation along with the size, this is now a two-stage shape evolution. As before, the plasma is always in contact with the outboard limiter. It starts with fixed elongation ($\kappa = 12$) and triangularity ($\delta = 0.2$). The size is increased until the final minor radius is reached (the width of the plasma fills the limiter). Only then are the elongation and triangularity increased to the final values. The break point is at 10.8 MA. As before, in all cases parameters are adjusted to make both the plasma energy and the current constant (not necessarily a stable equilibrium). The parameters for this case are shown in Fig. 4-2.

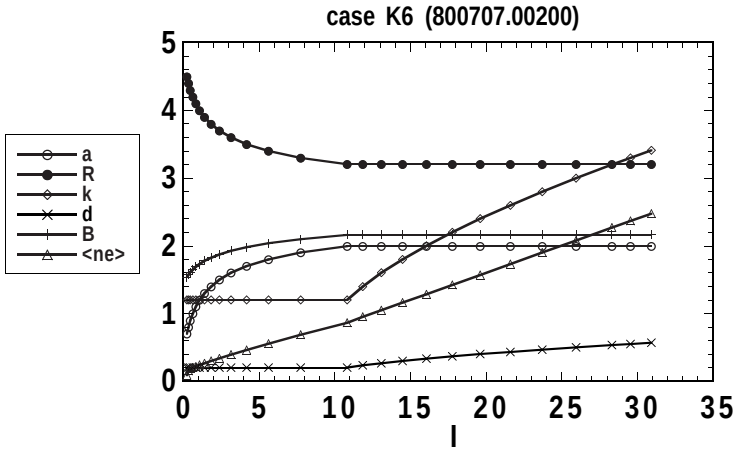

FIG. 4-2. Variation of shape parameters, magnetic field, and density as a function of current during ramp-up.

Two alternative variants were developed. Either the confinement is fixed at the level required for the final state (ordinary H–mode; $H97 = 1.051$; max $P_{NB} = 120$ MW), or the confinement multiplier is adjusted to keep the required heating power (100 kV deuterium beam) below 50 MW. The powers and H factors for these variants are shown in Figs. 4-3 and 4-4. In the spirit of assuming success, I propose using the $P_{NB} \leq 50$ MW variant.

As with the previous case, β_p never approaches the equilibrium limit, and β_N is a problem only at the lowest and highest current points (Fig. 4-5). (An arbitrary $\beta_N = 3$ limit was set for the small plasmas; see Fig. 4-6).

The final plot shows the current components (bootstrap and beam-driven) for the two variants. For the smaller plasmas, a significant level of external current drive is required.

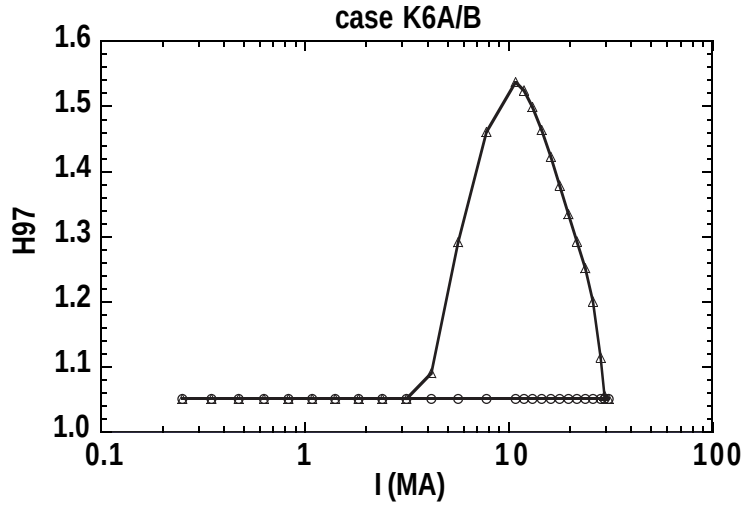

FIG. 4-3. Confinement factor increase (Δ) required for burn-control compared with unstable case with flat confinement factor (o).

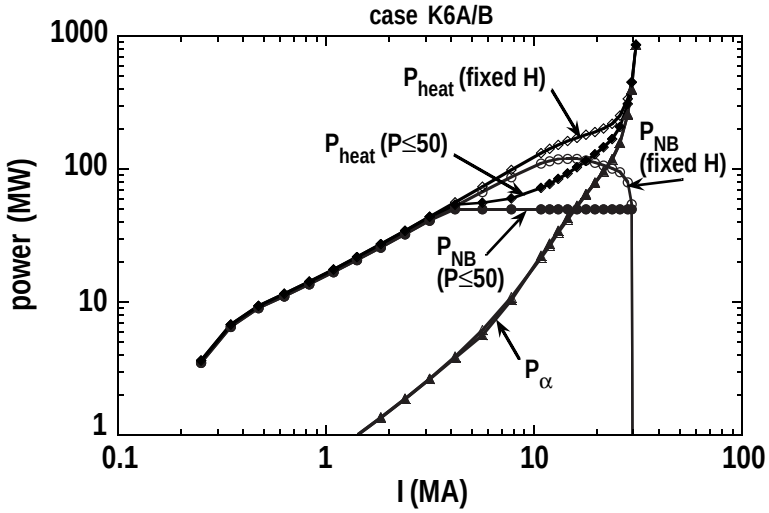

FIG. 4-4. Power requirements for fixed H versus adjusted H to keep power below 50 MW.

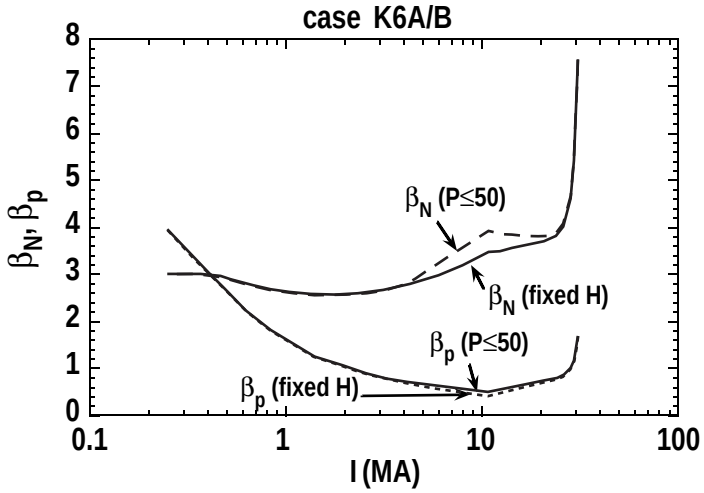

Fig. 4-5. β_N and β_p variation during current ramp-up.

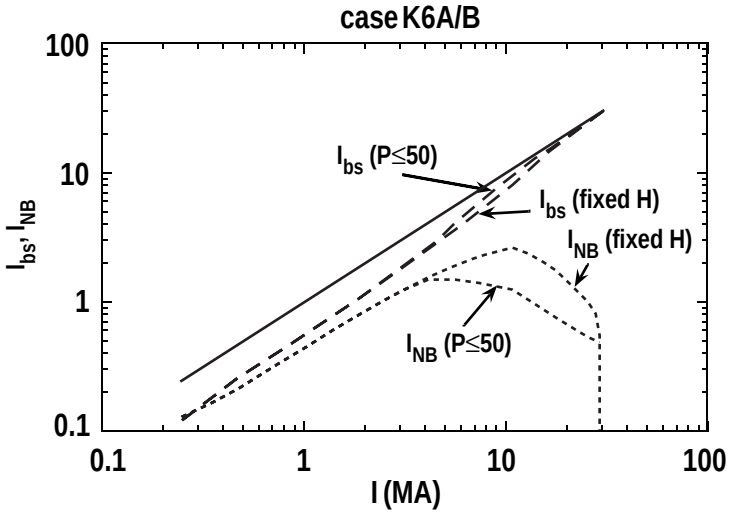

Fig. 4-6. Variation of bootstrap and neutral beam current for two confinement scenarios.

5. Prospects for Dealing with Scrape-off Layer Power Flows in ARIES-ST

5.1. Introduction

For the ARIES-ST tokamak to operate successfully, its divertor protective armor must be able to tolerate high heat loading. In the following discussion, we estimate the likely heat loads under ARIES-ST conditions and offer suggestions in how to handle these loads. In Section 5.2 we derive an expression for evaluating the peak heat flux in both inboard and outboard divertors. In Section 5.3 we estimate the peaked heat flux based on the present ARIES-ST design. In Section 5.4, we propose techniques to reduce excessive divertor heating. In Section 5.5, we discuss the problem of sputtering on the wetted surfaces. In Section 5.6, prospects for successful double-null ARIES-ST operation are examined.

5.2. Estimation of the Peaked Heat Flux

An exponential fall-off of the heat flux is assumed, that is

$$Q_{\text{div}} = Q_{\text{div},0} \times \exp\left\{-\frac{(R - R_0)}{f_{\text{exp}} \times \lambda_{\text{p}}}\right\} . \tag{5-1}$$

The power flow to the target is then

$$P_{\text{div}} = 2\pi \int_{R_0}^{\infty} \frac{Q_{\text{div}} \times R \times dR}{\sin\alpha} , \tag{5-2}$$

where P_{div} is the power flow at the target,
Q_{div} is the resulting heat flux distribution, such that:
$Q_{\text{div},0}$ is the peak heat flux at the divertor strike point,
R_0 is the major radius of the divertor strike point,
$R \geq R_0$,
I_{p} is the *midplane* heat flux scrape-off length,
f_{exp} is the flux expansion at the divertor target, and
α is the angle between the divertor incline and the separatrix.

Integrating Eq. (5-2) and simplifying the expression, we find

$$Q_{\text{div},0} = \frac{P_{\text{div}} \times \sin\alpha}{2\pi \times \mathrm{R}_0 \times f_{\text{exp}} \times \lambda_{\text{p}} \times \left\{1 + [(\mathrm{f}_{\text{exp}} \times \mathrm{l}_{\text{p}})/\mathrm{R}_0]\right\}} . \tag{5-3}$$

We estimate P_{div}

$$P_{\text{div}} \approx P_{\text{input}} \times (1 - f_{\text{rad}}) \times f_{\text{outboard/total}} \times f_{\text{gradB/total}} \times (1 - f_{\text{pfr}}) \ , \qquad (5\text{-}4)$$

where P_{input} is the total input power,
f_{rad} is the ratio of total radiated power to total input power,
$f_{\text{outboard/total}}$ ($f_{\text{inboard/total}}$) is the ratio of power flowing into the outboard scrape-off layer (SOL) to the power flowing into the outboard (inboard) SOL,
$f_{\text{gradB/total}}$ is the ratio of power striking the outboard divertor in the grad-B direction to the total power striking both upper and lower outboard divertors, and
f_{pfr} is the fraction of power flowing into the private flux region.

$$Q_{\text{div,0}} = \frac{P_{\text{input}} \times (1 - f_{\text{rad}}) \times \text{f}_{\text{outboard/total}} \times f_{\text{gradB/total}} \times (1 - f_{\text{pfr}}) \times \sin\alpha}{2\pi \times \text{R}_0 \times f_{\text{exp}} \times \lambda_{\text{p}} \times \left\{1 + [(\text{f}_{\text{exp}} \times \text{l}_{\text{p}}) / \text{R}_0]\right\}} \ . \qquad (5\text{-}5)$$

The peak heat flux predictions of Eq. (5-5) have been compared with DIII–D data and generally found to be within 20% of the measured peak heat flux.

5.3. Application to the ARIES-ST Peak Heat Flux Issue in the ‘‘Pure’’ DN Divertor Configuration

Because of the uncertainties in the boundary and SOL physics of high power, double-null divertors, care must be taken in applying Eq. (5-5). The mechanism (or mechanisms) responsible for determining SOL properties in double-null divertors are at present not well understood. Thus, it becomes necessary to look to data from present day double-null tokamaks for guidance. For example, for low triangularity double-null divertors in DIII–D operating at low to moderate density (*i.e.*, $\bar{n}_{\text{e}} / n_{\text{e}}$, Greenwald ≈ 0.5), the ratio of outboard : inboard power flow is typically $\approx 5:1$ and we will assume this power split is appropriate for ARIES-ST. In addition, the power scrape-off length λ_{p} must also be extrapolated; from DIII–D, λ_{p} at the *outboard* midplane is typically ≈ 1 cm. We have found experimentally that the λ_{p} at the *inboard* midplane is much less 1 cm and may, in fact, depend on toroidal field B_{T} and, based on available DIII–D data, we will assume that $\lambda_{\text{p}} \propto 1/B_{\text{T}}$.

The calculations below are based on the ARIES-ST "Strawman" parameters, listed in Table 5-1. In what we refer to as the ‘‘pure’’ double-null divertor option, the heat flows into both the upper and lower divertors and there is no significant plasma contact with any other vessel surfaces (*e.g.*, the centerpost). In estimating the peak heat flux under the outer divertor legs, we make the (pessimisitic) assumption that radiated power from the SOL and divertors are negligible. This gives us a ‘‘worst case’’ scenario. Using ‘‘Strawman’’ ARIES-ST parameters to determine the peak heat flux under the outboard divertor legs, that is, $P_{\text{input}} = 529$ MW, $f_{\text{rad}} = 0.45$, $f_{\text{outboard/total}} = 0.85$, $f_{\text{grad-B/total}} = 0.5$, $f_{\text{pfr}} = 0.10$, $f_{\text{rad}} = 0.45°$, $R_0 = 3.6$ m, $f_{\text{exp}} = 20$, and

Table 5-1
''Strawman'' parameters

	Inboard Leg(s)	Outboard Leg(s)
P_{input} (MW)	529	529
f_{rad}	0.45	0.45
λ_p	0.25	1.00
f_{exp}	20	20
f_{pfr}	0.1	0.1
R_0 (m)	1.8	3.6
Fraction of SOL power flow	0.15	0.85
$f_{grad\text{-}B/total}$	0.5	0.5
α (°)	90	90

$\lambda_{p,out} = 0.01$ m, we find that $Q_{div,0} \approx 16.5$ MW/m^2. Figure 5-1 shows how sensitive the peak heat flux is to: power input, incidence angle, midplane scrape-off length, and flux expansion.

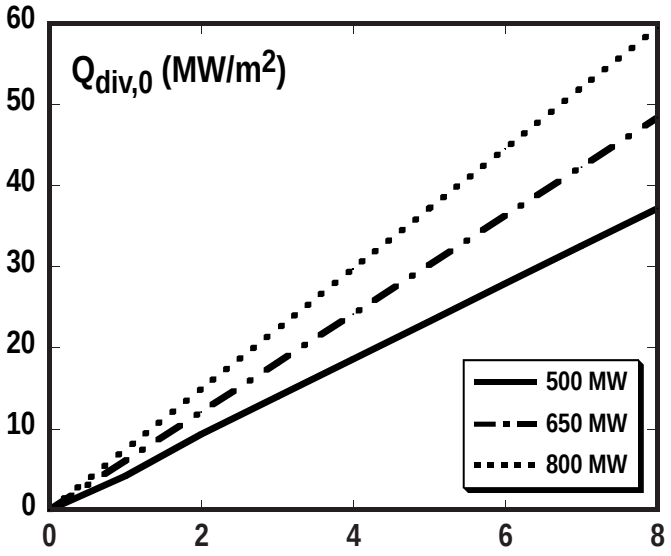

FIG. 5-1. Peak heat flux is plotted for three power input levels, as a function of α, λ_p, and f_{exp}. It is assumed that $f_{outboard/total} = 0.85$, $R_0 = 3.6$ m, and $f_{pfr} = 2$.

We can also give an upper bound to the peak heat flux to the tiles under the inboard divertor legs. The parameters we insert into Eq. (5-5) are the same as above, except $R_0 = 1.8$ m, $f_{inboard/total} = 0.15$, and $\lambda_{p,in} \approx 0.25$ cm. The peak heat flux under the inboard leg is: $Q_{div,0} \approx 31.3$ MW/m^2.

Both inboard and outboard heat flux are greater than what might be considered acceptable, that is, ≈ 10 MW/m^2. In Section 5-4 we propose solutions to how the peak heat flux values can be lowered to more manageable levels.

5.4. Two Methods for Reducing Peaked Heat Flux Values

While the peak heat fluxes to both the inboard and outboard divertors are fairly high, we think that these values can be reduced to more manageable levels by siphoning some of the SOL power to the centerpost and/or by shaping the divertors for more optimal handling of the power flow.

a. Sharing Power with the Centerpost

Experiments on DIII–D have demonstrated that energy confinement in (ELMing) H–mode plasmas is unchanged when the plasma is lightly limited on the centerpost and that this power is distributed (nearly) uniformly along the centerpost protective armor. In principle, if the double-null separatrix is lightly limited on the centerpost armor, the entire inboard power flow can be directed to the centerpost (and away from either inboard divertor). In the ''Strawman'' considered in this report, the total power flow along the inboard SOL would be ≈ 44 MW [*i.e.*, $P_{\text{input}} \times (1 - f_{\text{rad}}) \times f_{\text{inboard/total}} \approx 529\,\text{MW} \times (1 - 0.45) \times 0.15$]. Taking the wetted area on the centerpost as ≈ 75 m^2, we estimate that $Q_{\text{div,centerpost}} \approx 0.59$ MW/m^2. Because the value of average heat flux that the centerpost can handle has been set at 1.0 MW/m^2 and because approximately 0.56 MW/m^2 is already resulting from the (electromagnetic) radiated power from the core plasma, then ≈ 75% of the inboard SOL power (*i.e.*, ≈ 33 MW) can be directed to the centerpost armor. Thus, the power flow to the inboard divertors (≈ 11 MW) is much reduced and the separatrix-centerpost separation at the midplane can be small.

If the centerpost could accommodate a higher heat flux than 1 MW/m^2 (or if P_{input} were lower), it might be possible to (lightly) limit the separatrix on the centerpost armor. This might not only eliminate the power flow to the inboard divertors but also reduce the peak heat flux to the outboard divertors. Again, assuming the ''Strawman'' parameters and assuming an exponential scrape-off dependence of the heat flux, we find that peak heat flux in the outboard divertors can be lowered to ≈ 10 MW/m^2 with the average heat flux on the centerpost ≈ 2 MW/m^2. To do this, the flux surfaces outside the separatrix defined by R-$R_{\text{edge}} < 0.005$ m on the outboard midplane intersect the wetted centerpost, where R_{edge} is the radial coodinate of the separatrix at the outboard midplane. The flux surfaces on the midplane for $R - R_{\text{edge}} < 0.005$ m ''peel off'' into the outboard divertors.

b. Dissipating Power by Divertor Shaping

We can also reduce heat flux by making modest modifications on the divertor configuration such that the wetted area in the divertors is increased. The most practical way to do this is to reduce the angle α between the divertor incline and the separatrix. To

estimate value of α, such that $Q_{max,0}$ does not exceed 10 MW/m^2, we solve for α using Eq. (5-5). For the inboard divertors, $\alpha \leq 17°$; in the present configuration, $\alpha \approx 90°$. For the outboard divertors, $\alpha \leq 26°$; in the present configuration, $\alpha \approx 45°$.

5.5. Sputtering Concerns

While the heat flux appears manageable, the role of physical and chemical sputtering is much more problematical. Under high temperature plasma conditions, sputtering off the divertor plates can result in a contaminated core plasma and a significantly shortened lifetime for the plasma-exposed vessel components. The optimal material for the divertor plates (and centerpost plates) is still the subject of debate. However, regardless of the material that eventually will be selected, it will be important that the temperatures of the ion- and neutral particles striking that material surface be kept ''low.'' For example, tungsten, one of the candidates considered as a viable divertor material, appears to have favorable sputtering properties if the ion temperature at the strike points can be maintained ≤ 50 eV [5-1,5-2].

It is difficult to maintain an acceptably low ion temperature at the divertor strike points, if the ion temperature upstream (*e.g.*, on the midplane separatrix of the core plasma) is ''too high.'' We can estimate what these downstream and upstream temperatures might be along the outboard separatrix of the ARIES-ST ''Strawman,'' bearing in mind the uncertainties involved in this type of calculation. We follow the 1-D transport analysis developed by Barr and Logan [5-3]. We assume $T_e \approx T_i$ and that the midplane edge electron density is approximately 45×10^{20} m^{--3}. We find that $T_{i,div} \approx 60$ eV for the divertor and $T_{i,mid} \approx 95$ eV at the midplane separatrix. While these are only rough estimates, they do suggest that (1) the divertor ion temperature may not be too far off from an acceptable divertor operating temperature (*i.e.*, at least, for tungsten components), but that (2) the ion temperature on the midplane separatrix would be about a factor of two lower than the nominal ''Strawman'' value which is listed in the ''Strawman'' specifications at 200 eV.

In principle, this latter concern can be addressed either by lowering the midplane separatrix temperature by changing core plasma properties (*e.g.*, increasing radiated power from ''mantle'' of the core plasma) or by increasing the radiating properties of the SOL and divertors.

5.6. Conclusions

The peak heat flux on the inboard and outboard divertors for the 529 MW ''Strawman'' case has been estimated to be ≈ 31 and ≈ 16 MW/m^2, respectively. Both these values are well above the handling capabilities of present day cooling technology. These heat flux estimates may serve as an upper bound for ARIES-ST, because the radiated power outside the separatrix has not been considered here. Enhancing the radiating behavior of the SOL and divertor regions would ameliorate power flow at the divertor plates, although impurity ion transport in the SOL and divertors of the double-null configuration is somewhat speculative at present.

Two specific methods of reducing the peak flux have been outlined. The most straightforward of the two is tilting the wetted surfaces with respect to the divertor separatrix flux surface. The angles calculated to result in a peak heat flux of ≤ 10 MW/m^2 (*i.e.*, $\leq 17°$ and $\leq 26°$ for the inboard and outboard divertors, respectively) should not significantly complicate the divertor design.

The second method assumes that the double-null ARIES-ST core plasma can run close to (or on) the centerpost without an observable adverse effect on energy confinement. Moving the core plasma closer to the centerpost can reduce (perhaps, eliminate) power flow along the inboard SOL and, if the separatrix flux surface is limited on the centerpost, power flow to the outboard divertors also can be reduced. This method has been successfully tried in DIII–D for VH–mode operation [5-4]. This presupposes that plasma shape and location can be controlled sufficiently to do this. On the other hand, if the plasma control does result in the plasma leaning lightly on the centerpost armor, heat flux reduction on the inboard legs would be decreased ‘‘naturally.’’

Predicting the seriousness of the sputtering problem cannot be considered an isolated problem of only materials science or divertor physics. Minimizing the impact of material sputtering on divertor (or centerpost) protective plates depends on the kind of material used, the particle flux on the wetted surfaces, and the ion (and neutral particle) temperatures at the divertor plates. The latter two are affected by the divertor/SOL plasma (and neutral particle) transport and the plasma density and temperature upstream (*e.g.*, at the midplane separatrix). These, in turn, are affected by the transport properties of the core plasma. Our estimates of divertor and upstream (midplane) plasma density based on simple 1-D transport modeling suggest that plasma temperatures in the SOL and divertors are at least in a range that allows one to make a plausible argument for minimizing the effect of sputtering in ARIES-ST. A thorough study of the sputtering problem in an ARIES-ST type of tokamak, however, will require a much better understanding of double-null divertor and scrape-off physics and more sophisticated analysis tools.

References for Section 5

[5-1] W. Eckstein and J. Laszlo, J. Nucl. Mater. **183**, 19 (1991).

[5-2] C.H. Wu and U. Mszanowski, J. Nucl. Mater. **218**, 293 (1995).

[5-3] W.L. Barr and B.G. Logan, Fusion Technol. **18**, 251 (1990).

[5-4] G.L. Jackson, T.S. Taylor, C.J. Lasnier, *et. al.*, Phys. Plasmas **3**, 1005 (1996).